PLANT SCIENCE TODAY
Vol 12(sp4): 01–13
https://doi.org/10.14719/pst.8380

eISSN 2348-1900

RESEARCH ARTICLE

# Detection of nutrient deficiency in plants using radial basis function neural network with a modified adaptive Kalman filter

**Anish Sathyan*** **& P Palanisamy**

Department of Electronics and Communication Engineering, National Institute of Technology, Trichy 620 015, Tamil Nadu, India

*Correspondence email - satyan@cdac.in

Received: 19 March 2025; Accepted: 26 July 2025; Available online: Version 1.0: 23 October 2025

**Cite this article:** Anish S, Palanisamy P. Detection of nutrient deficiency in plants using radial basis function neural network with a modified adaptive Kalman filter. Plant Science Today. 2025;12(sp4): 01–13 https:/doi.org/10.14719/pst.8380

## Abstract

The agriculture sector plays a significant role in the national GDP. *Global agricultural industries employ advanced techniques for the early detection and characterisation of plant nutrient deficiencies to enhance crop yield*. In most agriculture-dependent countries, economic growth is determined by the gross yield of entire plantations. Plants exhibit noticeable symptoms such as changes in leaf colouration, spotting, or altered growth patterns. These symptoms, including yellowing (chlorosis), browning, or stunted growth, indicate potential nutrient deficiencies. Monitoring these variations enables early detection of deficiencies before they significantly affect plant health. Early detection of nutrient deficiencies plays a pivotal role in achieving a speedy recovery from the disease, thereby assuring sufficient improvement in the plant's yield. This article proposes a method for the early detection of nutrient deficiency in plants based on variations in leaf colour and pattern. It uses 54305 data points with three versions of the same images, differing in colour, greyscale and segmentation. Initially, image preprocessing is carried out using Fuzzy Histogram Equalization (FHE) and a modified adaptive Kalman filter to achieve better results. The pre-processed image datasets are then used to train the proposed Radial Basis Function Neural Network (RBFNN). The proposed RBFNN model demonstrates significant improvements (1.18-16.47 %) in accuracy, precision, specificity, sensitivity and F-score compared to conventional models.

**Keywords:** fuzzy histogram equalization; histogram equalisation; Kalman filter; neural networks; nutrient deficiency; radial basis function neural network (RBFNN)

## Introduction

Computers embedded with novel algorithms can process information from stored images, which play a vital role in many fields such as defence, engineering, agriculture and medicine (1). An image may contain valuable information which can be recovered with the help of some computational techniques. The process of partitioning a given image into meaningful smaller parts is known as image segmentation. Image segmentation is mainly applied on common objects appearing in an image. Image processing can be performed using two common methods: conventional and soft computing. Thresholding, edge-based and region-based techniques are used in the conventional method. Uncertainty in image segmentation is dealt by the soft computing method. Human intelligence is simulated using soft computing methods, which learn human skills and enable machines to perform complex tasks automatically. Soft computing is a group of methods that includes particle swarm optimization, fuzzy logic, bacterial foraging optimization, neural network, swarm intelligence and genetic algorithms.

Plants are an important part of human ecological system. It plays an important role in the life of human beings. They are the backbone in maintaining a balanced environment. Like human beings, plants suffer from diseases. These diseases affect plants in various ways, such as stunted growth, pale leaves and dry stems (2). Nutrient deficiency also causes severe deformation in plant growth and yield. Detecting and curing plant deformities in time is an important task. Skilled human intervention is required to detect, identify and classify diseases. The major drawback of this method is the lack of adequate expertise and the time it consumes. An expert can identify and classify nutrient deficiencies with the naked eye, but it requires a lot of time. The process takes longer and makes the task cumbersome. By applying soft computing techniques, an automated monitoring system can be applied for the early detection and identification of patterns that develop on plant leaves due to nutrient deficiency. This is a beneficial and cost-effective approach to identifying and classifying nutrient deficiency syndromes in plants at an early stage. Tackling algorithms have been proposed for identifying nutrient deficiencies in plants using proximal images. These algorithms analyze visible symptoms such as leaf colour changes, shape distortions and texture anomalies to detect specific deficiencies (e.g., nitrogen, phosphorus, potassium, etc.).

### Related works

RGB sensors, multispectral sensors and hyperspectral sensors are used for capturing images at close range for the database, which will be used for machine learning (3). This article discusses

mineral deficiency in plants. The authors have expanded their focus beyond nitrogen to include other minerals. Mineral deficiency is identified by reflectance spectroscopy. Different characteristic symptoms, such as interveinal chlorosis in young leaves, chlorosis starting from older leaves, marginal chlorosis followed by necrosis and interveinal chlorosis on older leaves indicate deficiencies of minerals like iron (Fe), nitrogen (N), potassium (K) and magnesium (Mg). In the projected technique, chlorotic symptoms are suggested for identifying the deficiency (6). The neural network-bacterial foraging approach is carried out to deliver optimal weights for identifying plant nutrient deficiency using leaf images. A region-growing-based algorithm is used to improve the efficiency of feature extraction and classify the infected region. The described technique demonstrates success in both identification and computational efficiency (7). The authors have taken maize to identify nitrogen deficiency. A simple learning-based approach is derived from a pre-trained CNN model for analysis (8). Deficiency of nitrogen in oil palm tree is discussed in this paper. Leaf surfaces are captured with high-end digital camera for identifying the deficiency. Further, feature extraction is carried out for texture, shape and colour. The output of the extraction is fed to fuzzy classifier (9). Nitrogen deficiency in maize has been reported by a previous study (11). New method is adapted for it. The Artificial Vision System (AVS) is used for analysis, especially during the early stages. Methods like Volumetric Fractional Dimension (VFD) and Gabor Wavelets (GW) are included in Automated Visual Systems. VFD is a texture analysis method based on fractal geometry and GW is a set of filters used to extract texture, orientation and frequency information from images. As a result, it is stated that GW is the best method for feature extraction for colour images. All this is carried out for green house vegetation.

In a previous study, six macronutrient deficiencies in plants were discussed and the important nutrients used for plant growth are N, P, K, calcium (Ca), sulphur (S) and Mg (12). An automated solution was provided by creating a database of both healthy and defective leaves (12). This database was then used in machine learning for the identification of nutrient deficiencies. Deficiency of N in corn fields was detected using high-resolution images. Unmanned aerial vehicles were employed to capture images from the crop fields, which were then processed in a systematic pipeline. This approach improved the efficiency of N-deficiency detection compared to the conventional techniques (13). Fig. 1 portrays sample healthy and N-deficient leaf images clearly showing that colour distribution determines leaf health, whereas Fig. 2 illustrates a possible distribution of N-deficient leaves versus N-treatment using fertilizers across a typical corn field. As the rate of fertilizer treatment increases, after a certain point, the overall distribution of N-deficient leaves decreases and healthy leaves are generated throughout the field.

A novel technique is proposed to estimate the true chlorophyll level or nutrient content, which cannot be directly observed, as well as incomplete image data caused by occlusion during measurement. This study discusses noise covariance matrices in discrete-time invariant systems with additive White Gaussian noise, analyzed using a linear Kalman filter (14). When process and measurement noise covariance matrices are inaccurate, solving the filtering problem for a linear Gaussian state-space model was the focus of an earlier study (15). A new variational Bayesian (VB)-based adaptive Kalman filter (VBAKF) with inaccurate process and measurement noise covariance matrices, along with a predicted error covariance matrix, was proposed using inverse Wishart priors for inference. This method provides improved robustness to resist the uncertainties of covariance matrices compared to existing filters. A set of enhancement stages used for improving finger vein images offers high distinctive power and low computational complexity. In this methodology, the enhancement stages are positioned around fuzzy histogram equalization. The evaluation is carried out by two sets: one with the distinctive approach, formulated by reorganizing and collecting the preprocessing steps of the

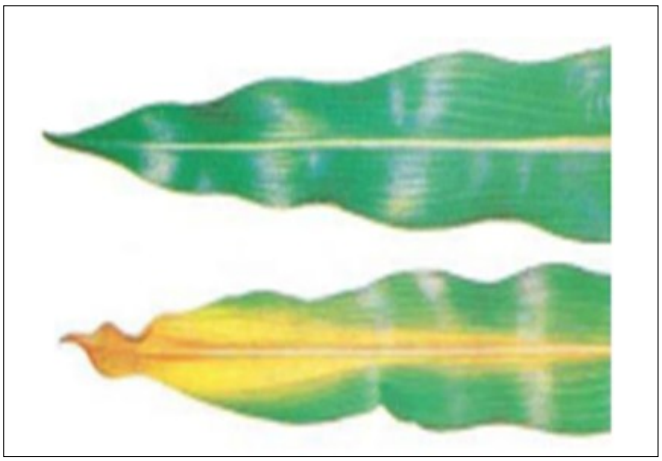

**Fig. 1.** Sample healthy (top) leaf and N-deficient (bottom) leaf images.

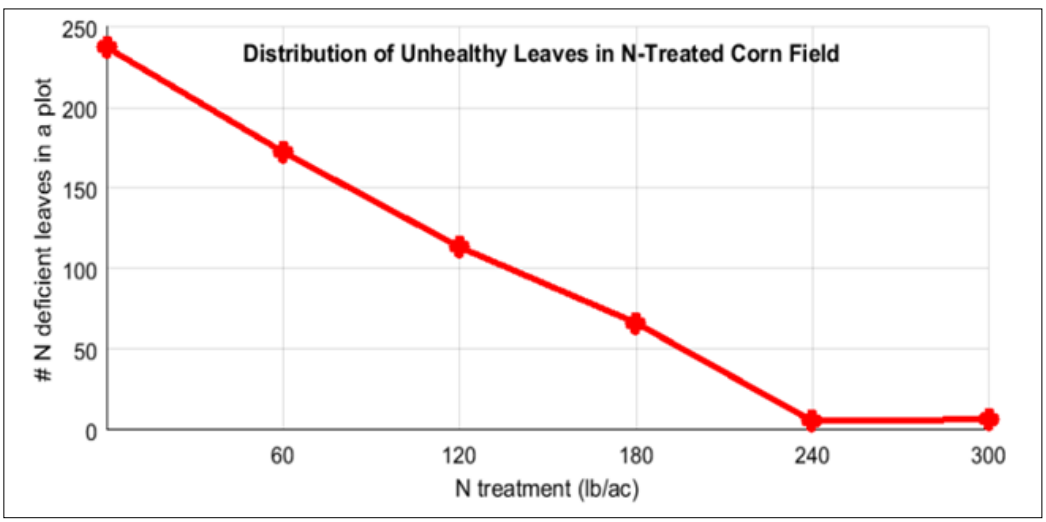


**Fig. 2.** Relationship between N-treatment and N-deficiency.

unique projected method and another with the proposed approach. To extract the characteristics, a combination of Gradient Histogram and Hierarchical Centroid was used. Both the improvement stages were evaluated using Deep Neural Networks and K-Nearest Neighbour, utilizing six-fold stratified cross-validation. Experimental results of this method show improvements compared to three newest benchmarks that also used six-fold validation (16).

By using fuzzy clustering, the histogram of the original image was divided into three sub-histograms (17). The acquired sub-histograms were biased based on the inference from the Fuzzy Mamdani system and afterward they were combined to produce a different histogram. The created histogram was adjusted to minimize the unwanted effects of pits and spikes. Finally, using equalization, an improved image was obtained from the reformed histogram image. The Fuzzy inference system with Mamdani method allocates suitable dynamic ranges to every input interval for the sub-histograms of gray levels, thereby improving the image details. For image contrast enhancement, fuzzy logic-based histogram equalization (FHE) is proposed in previous research (18). The FHE is superior to conventional histogram equalization because it handles uncertainty and image ambiguity more effectively. The FHE comprises dual phases. In the initial phase, based on fuzzy set theory, the fuzzy histogram is calculated to better address the uncertainty values of gray levels compared to conventional crisp histograms. In the next phase, based on the average value of the new image, the fuzzy histogram is classified into two sub-histograms, which are then balanced individually to preserve the brightness of the image.

The quantitative and qualitative analyses of the FHE algorithm are assessed using two familiar factors: natural image quality evaluator (NIQE) and average information content (AIC) for different images. It is exciting to realize from the quantitative and qualitative measures that the proposed technique affords optimal outcomes by getting improved contrast enrichment as well as conserving the native data of the original image. This analysis reveals that the technique significantly and effectively eradicates the exhausted presence and opposes the noise made by numerous existing techniques.

Replacing standard convolution with depth-wise separable convolution reduces parameter count and computational cost (20). Depth-wise separable convolution drastically reduces model size and computation by factorizing standard convolution into two simpler steps-depth-wise and point-wise-without significantly compromising accuracy. The open dataset was trained on the executed models containing fourteen plant classes, as well as healthy plant leaves and thirty-eight categorical disease classes. The features of leaves such as batch size, number of iterations and dropout were integrated to estimate the performance. This model has obtained a classification accuracy rate of 99.56 %, 97.02 %, 99.11 % and 98.42 % using EfficientNetB0, MobileNetV2, InceptionResNetV2 and InceptionV3 respectively. These accuracy values are better than those of conventional characteristics-based methods. Compared with other existing methods, this proposed method attained improved accuracy, but it takes longer time for training the system (21). This work classifies two plant diseases-early blight and late blight-using potato leaf images from the PlantVillage dataset. The features are extracted using the Gray Level Co-occurrence Matrix (GLCM). After feature extraction, the images are classified using a Support Vector Machine (SVM). This model achieved an accuracy of 92 %. The authors proposed a system to predict plant disease in the leaf images using an RBFNN, with the dataset collected from database repository of IPM Agriculture. This also achieved better performance in terms of prediction accuracy (22). An improved real-time application is proposed, like a human brain computer interface implemented in video gaming, by using adaptive Kalman filter (AKF). To reduce the effect of missing frames and to estimate motion information, the adaptive Kalman filter is used to get better performance (23). The author identified plant disease using a histogram matching algorithm, with the help of edge detection techniques and colour features to predict the disease in plant leaves (24).

In DIP_DLND, a 23-layer deep learning technique was proposed to identify plant stress levels caused by N deficiency. A 23-layer CNN handles complex tasks across different domains, highlighting its capability to learn deep hierarchical features and deliver high accuracy in classification and detection tasks. Stress was classified based on the phenotyping approach. A comparison of conventional deep learning algorithms like ResNet18 and NasNet Large was made and the proposed DL algorithm showed an accuracy of 8.25 % higher than the conventional algorithms (4). DIP_CRND deals with hyperspectral imaging for identifying N deficiency in soilless tomato crops. The analysis was conducted under controlled conditions, where N deficiency was observed to impact the intensity of spectral reflection. Parameters used for calculating the deficiency include leaf chlorophyll and leaf photosynthesis rate. In addition, the photochemical reflectance index (PRI) and the transformed chlorophyll absorption in reflectance index (TCARI) were identified to carry out deficiency calculations. A spectral index was also developed for evaluating nitrogen concentration (5).

DIP_SEMSI deals with N deficiency in corn plants with site -specific yield. The study employed multispectral imaging using both ground-based and aerial data. The proposed method estimated the shadow effect on the required images and the analysis was based on canopy reflectance. The results were evaluated using the NDVI and NIR channels. The database of canopy images was compiled under various light positions. Soil Plant Analysis Development (SPAD) meter readings were also considered as parameters (10). Random capture and scanning of rice leaves were utilized to investigate the varying nature of leaf features under nutrient stress. Leaf features were calculated by average values as well as by the functions of region props in MATLAB and then the dynamics of leaves were enumerated by estimating the rate of relative growth. Stepwise discriminant analysis and leaf-one-out cross-validation were used to find NPK deficiencies. The experimental results showed that N-deficient leaves exhibited the smallest rate of extension and the fastest rate of wilt, followed by P and K-deficient leaves. Throughout the documentation, both colour indices and the morphological traits of the initially inadequate leaves were the actual indices for verification. Furthermore, the first inadequate leave had relative benefit in early diagnosis (validation accuracy of 71.4 %, training accuracy of 73.7 % after the 26$^{th}$ day of transplantation) and the third completely extended leaves produced greater accuracy at future phases (19).

## Limitations of related works

A well-structured strategic optimization model is needed to enhance performance, as some existing models fail to achieve reliable and sufficiently high prediction accuracy. In order to improve accuracy, well-defined preprocessing models must be identified, which are not widely seen in the early literature.

## Proposed model

In this work, before training the RBFNN, the dataset containing 54305 images underwent processing using FHE to extract the features. These extracted features are then fed into the Modified Adaptive Kalman filter to effectively eliminate noise components. Fig. 3 depicts the proposed flow diagram illustrating the use of RBFNN in the study. Subsequently, the proposed RBFNN is trained using 70 % of the dataset and the remaining 30 % is used to test the neural network. As a result, the RBFNN predicts the nutrient deficiency of the test plant leaves with high accuracy using fast computations.

The following steps are used to determine the nutrients of the plant:

### 4.1. Fuzzy Histogram Equalization (FHE)

FHE preserves image brightness while ensuring that histogram peak mappings are not repeated. The flow diagram in Fig. 4 depicts the method adopted for FHE. The histogram values are redistributed uniformly between valley-like areas of consecutive peaks.

Fuzzy histogram is normally defined by a sequence of real numbers

$$h_1(i); i \in \{0,1,\ldots,L-1\} \qquad \text{(Eqn. 1)}$$

Where, the frequency $h_1(i)$ indicates the occurrence of gray levels at i Gray values are represented as I (x,y) with a fuzzy number I ‘ (x, y)

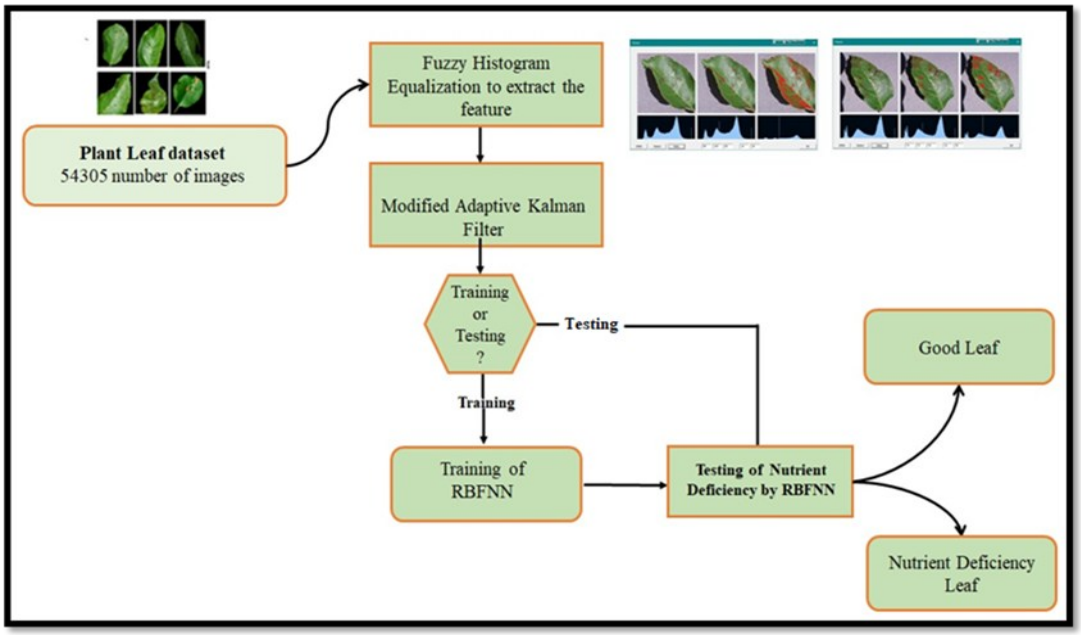


**Fig. 3.** Flow diagram of the proposed RBFNN.

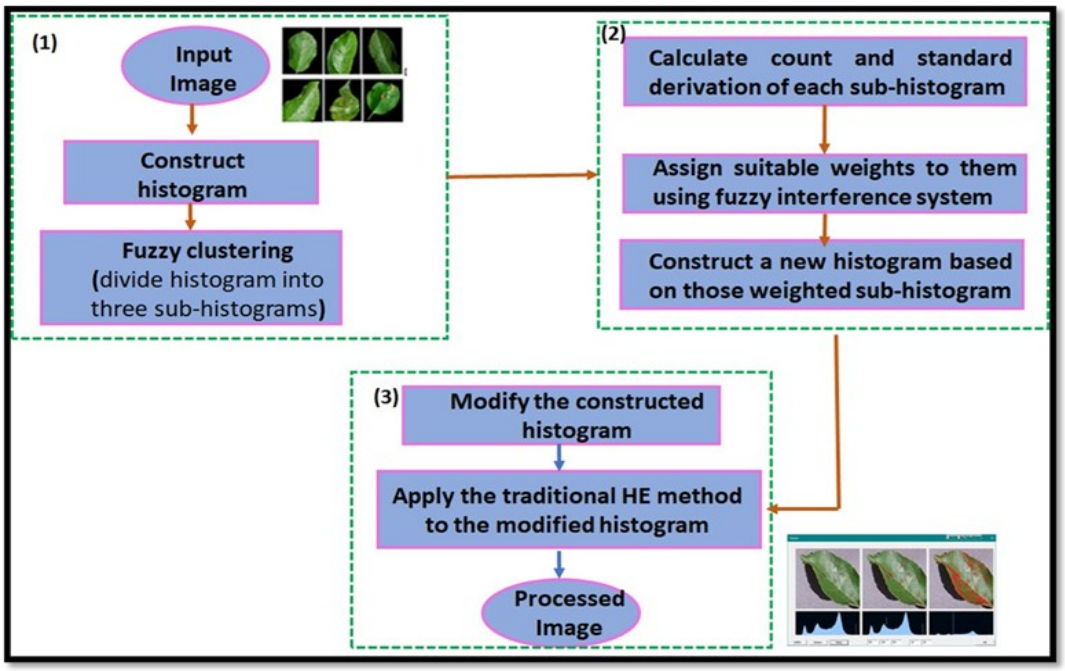


**Fig. 4.** Flow diagram of Fuzzy Histogram Equalization.

Then the fuzzy histogram is given by

$$h_1(i) \leftarrow h_1(1) + \sum_x \sum_y \mu I'(x,y)i \quad k \leftarrow [a,b] \qquad \text{(Eqn. 2)}$$

$$\mu I'(x,y)i = \max\left(0{,}1 - \frac{|I(x,\ y) - i|}{4}\right) \qquad \text{(Eqn. 3)}$$

Where, (a, b) are support values of fuzzy membership function.

Steps involved:

i) Get the real numbers of the corresponding image

ii) Find the I(x, y)

iii) Find the I'(x, y)

iv) Find the fuzzy triangular value μI'(x,y)

v) Find the h(i)

The performance impact of the proposed FHE method on some sample images is depicted in Fig. 5.

**4.2. Modified Adaptive Kalman Filter (MAKF)**

MAKF with inaccurate measurement noise and process covariance matrices is proposed for linear state-space Gaussian models. Using the adapted method with inverse Wishart priors, the state estimation accounts for both measurement noise and predicted error covariance matrices. MAKF demonstrated greater robustness against uncertainties in measurement noise and process covariance matrices compared to existing state-of-the-art filters. MAKF consists of two processing stages, namely prediction and updating.

**4.2.1. Prediction stage:** Initialize $m_0$, $p_0$, $v_0$ and $\varepsilon_0$ parameters of mean and covariance; $L_k$, $C_k$ and $N_k$ are known matrices and $V_k$ and $V_k$ are parameters of inverse Wishart distribution.

1. Take K=1, 2… perform the steps given below

2. Do $mk = C_k m_{k-1}$

$$P_k = C_k P_{k-1} C_K^T + L_k$$

$$v_k = \varepsilon(v_{k-1} - n - 1) + n + 1$$

$$V_k = D V_{k-1} D^T$$

**4.2.2. Updating stage:** 1. Take i = 1, 2,…, N

$$S_K^{i+1} = N_K P_K N_K^T + (v_k - N - 1)^{-1} V_k^i$$

$$K_K^{i+1} = P_K N_K^T (S_K^{i+1})^{-1}$$

$$m_K^{i+1} = m_k + K_k^{i+1}(Y_K - H_K m_K)$$

$$P_K^{i+1} = P_K - K_k^{i+1} S_K^{i+1} (K_K^{i+1})^T$$

$$V_K^{i+1} = V_k - N_K P_K^i N_K^T (Y_K - N_K m_K^i)(Y_K - N_K m_K^i)^T$$

**4.3. Radial Basis Function Neural Network (RBFNN)**

RBFNN is one of the machine learning algorithms that is extremely fast, effective and intuitive. It consists of three layers and can be applied to both regression and classification problems.

The RBFNN structure containing the input, hidden and output layers is shown in Fig. 6. In this work k-means clustering along with linear regression is used to classify the images. The RBF yields information about the confidence rate of prediction.

To get a smooth transition, the negative squared Euclidean distance is multiplied by a scalar coefficient, Beta. Applying the exponential function to that multiplication value helps to control how fast the function will decay. In fact, the value of Beta parameter decides the smooth transition so that small beta value produces a wide response and high value of Beta induces a sharper decline of the function curve. Smooth transition (st) is represented as in Equation 4.

$$st = e^{-\beta L^2} \qquad \text{(Eqn. 4)}$$

β - Beta, the hyperparameter

L - Distance between centroids

Beta should be fine-tuned to get better result. In this work, 2 options are tried to compute the Beta value. First option is taking standard deviation of the cluster

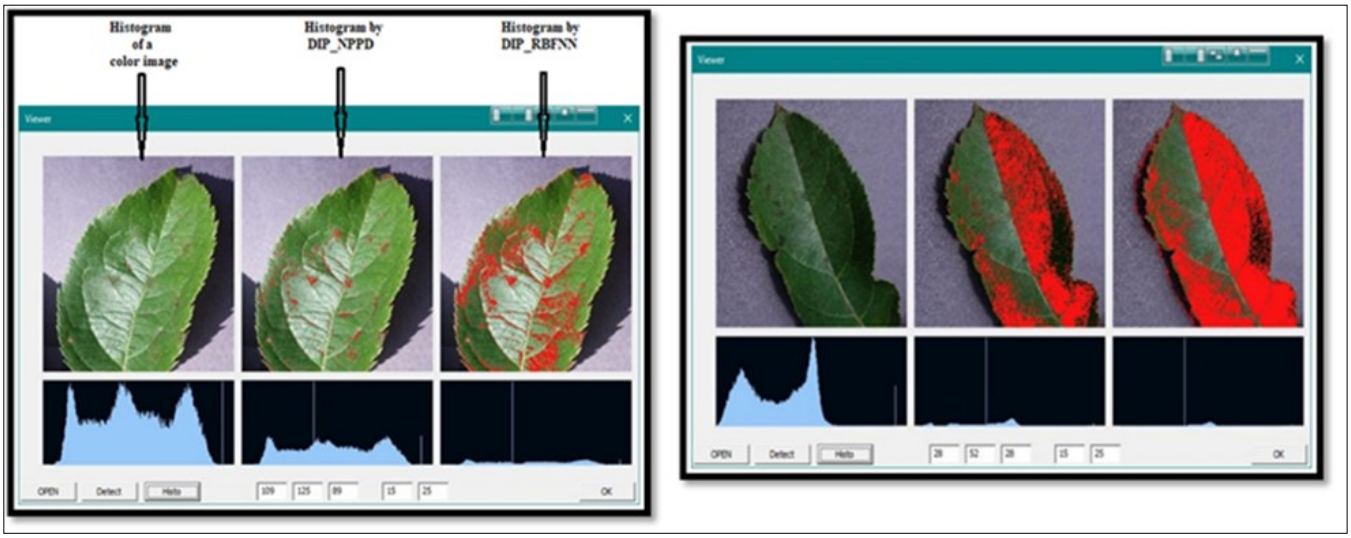


**Fig. 5.** Effect of FHE on sample images.

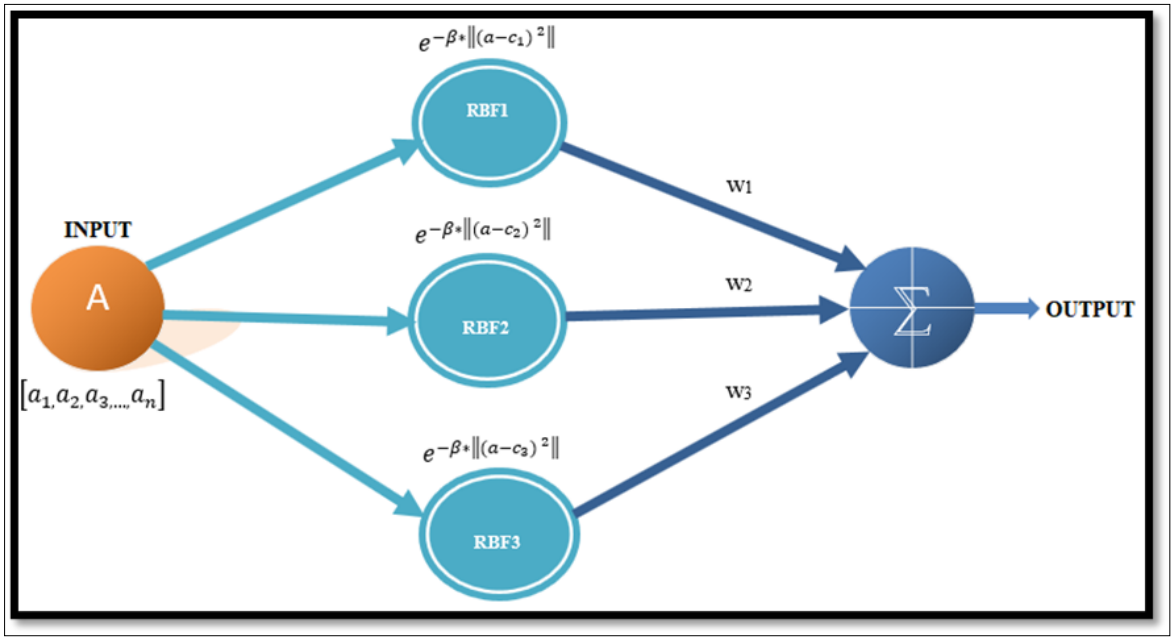


**Fig. 6.** Radial Basis Function Neural Network (RBFNN) model.

$$\beta = \frac{1}{sd^2} \qquad \text{(Eqn. 5)}$$

Sd - standard deviation

Second option is also applicable to derive β using the following alternative Equation 6.

$$\beta = \frac{\sqrt{2 * N}}{L_{MAX}} \qquad \text{(Eqn. 6)}$$

Where, N is the number of centroids and $L_{MAX}$ is the maximum distance between any two centroids.

Using Pythagoras theorem one can easily find the Euclidian distance L as in Equation 7.

$$L = \|a - c\| = \sqrt{(a_1 - c_1)^2 + (a_2 - c_2)^2 + \cdots + (a_n - c_n)^2}$$

(Eqn. 7)

$[a_1,a_2,a_3,\ldots,a_n]$ – Input vector

$[c_1,c_2,c_3,\ldots,c_n]$ – Centroid vector

**Optimisation:** Here, Least Squares Linear Regression (LSLR) is used to find the weights. LSLR assigns different learning rates to different layers rather than using a single global learning rate. LSLR ensures a balanced and adaptive approach by scaling learning rates per layer, leading to better training dynamics and performance, especially in deep or pretrained models, compared to using a single uniform learning rate across all weights. The global minimum of the cost function can be calculated in a short time using LSLR compared to Cyclical Learning Rates (CLR), Layer-wise Adaptive Rate Scaling (LARS) and Layer-wise Learning Rate Decay (LLRD). The final output is the minimum weight, as mentioned in Equation 8.

$$w = (V^T V)^{-1} V^T O \qquad \text{(Eqn. 8)}$$

From the above equation, the image classification problem V is a 2-dimensional matrix of RBF and O is the one-hot encoded 2-dimensional matrix. The following steps are needed to predict the unknown point:

1. Need to get the RBF of an unknown data point with respect to all centroids.
2. Calculate dot product of W and RBF by selecting an index of maximum value.

## Results and Discussion

### Leaf image dataset

The PlantVillage dataset along with IPINI dataset is used for training and testing purposes, containing more than 55000 healthy, nutrient-deficient and disease-infected images of plant leaves. In this database, 14 different types of plant leaves are available with 38 different classes, such as distinct species, condition status, leaf ages and environmental conditions. All images are captured and pre-processed in a highly equipped laboratory setting. Three different formats of plant datasets are used in the proposed experiment. Of the total datasets, 70 % are used for training the network and the remaining 30 % are used for testing.

### Performance analysis metrics

Accuracy, precision, specificity, sensitivity, F-score and average processing time are used to measure the performance of the proposed RBFNN. The PlantVillage dataset of colour, grayscale and segmented images is divided into 10 data chunks and each data chunk has 10 % of the total 2 GB images. The entire dataset was processed using existing methods like DIP_DLND, DIP_CRND, DIP_SEMSI, DIP_NPPD and then compared with the outcome of the proposed DIP_RBFNN method.

$$\text{Accuracy in \%} = \frac{\text{True positive} + \text{True negative}}{\text{Total}} \times 100$$

$$\text{Precision in \%} = \frac{\text{True positive}}{\text{Predicted}} \times 100$$

$$\text{Specificity in \%} = \frac{\text{True negative}}{\text{False positive} + \text{True negative}} \times 100$$

$$\text{Sensitivity in \%} = \frac{\text{True positive}}{\text{True positive} + \text{False negative}} \times 100$$

$$\text{F} - \text{score in \%} = \left(2 \times \frac{\text{Precision} \times \text{Sensitivity}}{\text{Precision} + \text{Sensitivity}}\right) \times 100$$

From Table 1 and Fig. 7, it is observed that when the data chunk crosses above 70 %, the accuracy of proposed method (DIP_RBFNN) improves by 8.90 % compared to DIP_DLND, 16.34 % compared to DIP_CRND, 10.69 % compared to DIP_SEMSI and 1.23 % compared to DIP_NPPD for the PlantVillage dataset.

As shown in Table 2 and Fig. 8, it is observed that when the data chunk crosses above 70 %, the precision of proposed method (DIP_RBFNN) improves by 8.81 % compared to the DIP_DLND, 16.46 % compared to DIP_CRND, 10.26 % compared to DIP_SEMSI and 1.30 % compared to DIP_NPPD for the PlantVillage dataset.

As shown in Table 3 and Fig. 9, it is observed that when the data chunk exceeds 70 %, the sensitivity of the proposed method (DIP_RBFNN) improves by 9.00 % compared to the DIP_DLND, 16.28 % compared to DIP_CRND, 11.05 % compared to DIP_SEMSI and 1.18 % compared to DIP_NPPD for the PlantVillage dataset.

As shown in Table 4 and Fig. 10, it is observed that when the data chunk crosses 70 %, the specificity of the proposed method (DIP_RBFNN) improves by 8.80 % compared to the DIP_DLND, 16.39 % compared to DIP_CRND, 10.33 % compared to DIP_SEMSI and 1.27 % compared to DIP_NPPD for the PlantVillage dataset.

**Table 1.** Experimental accuracy (%)

| Data (%) | DIP_DLND | DIP_CRND | DIP_SEMSI | DIP_NPPD | DIP_RBFNN |
|---|---|---|---|---|---|
| 10 | 55.849998 | 45.542274 | 47.510906 | 63.592648 | 53.092648 |
| 20 | 66.585022 | 57.53244 | 60.404171 | 73.827667 | 66.940025 |
| 30 | 72.822121 | 64.150002 | 67.300003 | 79.564774 | 75.04023 |
| 40 | 76.820038 | 69.022614 | 73.047432 | 83.562691 | 80.787407 |
| 50 | 80.364975 | 72.552101 | 76.617653 | 86.857628 | 85.24527 |
| 60 | 82.557144 | 75.390167 | 79.94326 | 89.799789 | 88.887604 |
| 70 | 85.083336 | 78.251099 | 83.00502 | 91.575981 | 92.467155 |
| 80 | 86.555061 | 80.262779 | 84.690689 | 93.797707 | 94.134789 |
| 90 | 88.79425 | 83.007729 | 86.839096 | 95.786896 | 97.487801 |
| 100 | 90.099998 | 83.792267 | 89.76091 | 97.342651 | 99.092651 |

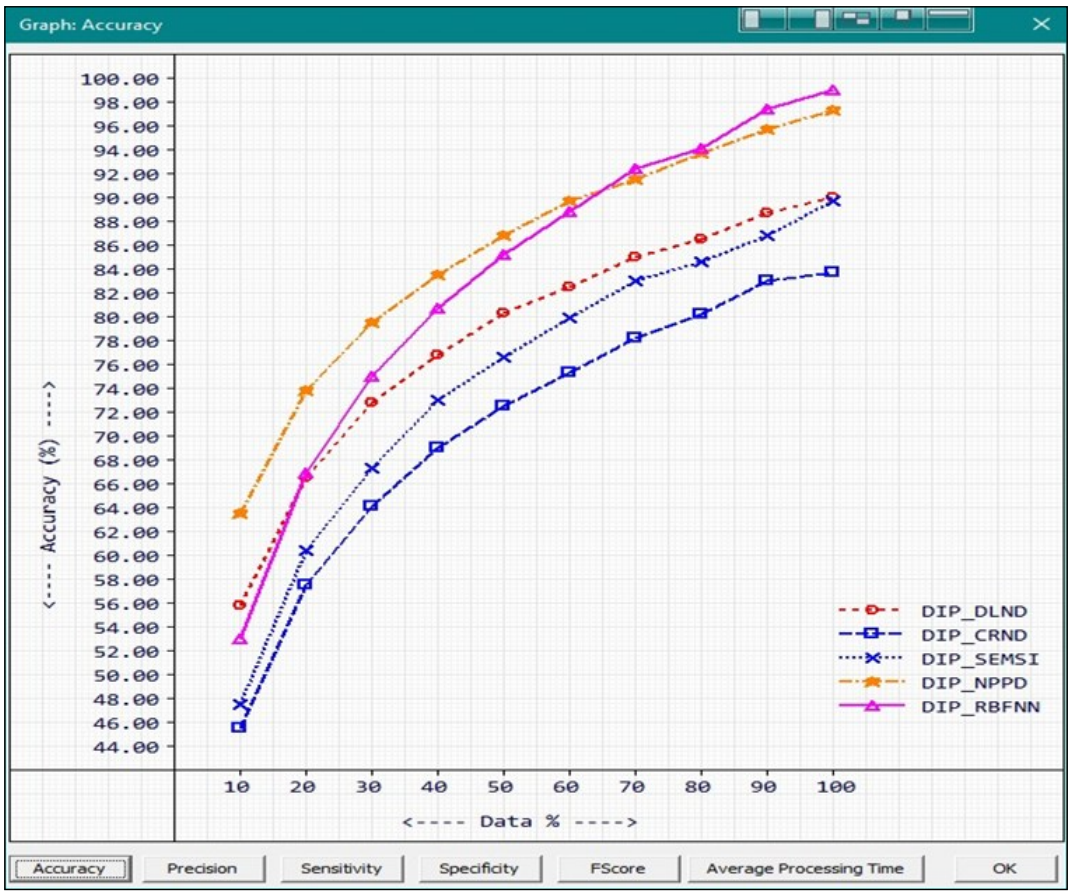


**Fig. 7.** Accuracy chart.

**Table 2.** Experimental precision (%)

| Data (%) | DIP_DLND | DIP_CRND | DIP_SEMSI | DIP_NPPD | DIP_RBFNN |
|---|---|---|---|---|---|
| 10 | 56 | 45.892273 | 47.960907 | 63.592648 | 52.592648 |
| 20 | 67.235023 | 57.132442 | 60.604168 | 73.827667 | 67.440025 |
| 30 | 73.722122 | 63.5 | 67 | 79.814774 | 74.54023 |
| 40 | 76.470039 | 68.372612 | 72.747429 | 84.062691 | 81.287407 |
| 50 | 80.264977 | 72.1521 | 76.31765 | 86.357628 | 84.74527 |
| 60 | 82.957146 | 75.740173 | 80.643257 | 90.049789 | 89.387604 |
| 70 | 84.73333 | 78.851097 | 82.955025 | 91.325981 | 92.467155 |
| 80 | 86.705063 | 79.612778 | 84.890686 | 93.297707 | 94.134789 |
| 90 | 88.444244 | 82.607727 | 87.039093 | 96.036896 | 97.487801 |
| 100 | 90.5 | 83.392273 | 90.460907 | 97.092651 | 98.592651 |


**Fig. 8.** Precision chart.

**Table 3.** Experimental sensitivity (%)

| Data (%) | DIP_DLND | DIP_CRND | DIP_SEMSI | DIP_NPPD | DIP_RBFNN |
|---|---|---|---|---|---|
| 10 | 55.8325 | 45.573261 | 47.533108 | 63.592648 | 53.123886 |
| 20 | 66.372185 | 57.593189 | 60.362713 | 73.827667 | 66.772301 |
| 30 | 72.418587 | 64.33638 | 67.404427 | 79.417686 | 75.293159 |
| 40 | 77.009102 | 69.273163 | 73.186546 | 83.230385 | 80.482574 |
| 50 | 80.425835 | 72.733978 | 76.77832 | 87.229927 | 85.60128 |
| 60 | 82.298752 | 75.213676 | 79.529846 | 89.601776 | 88.502579 |
| 70 | 85.33065 | 77.9161 | 83.038063 | 91.784904 | 92.467155 |
| 80 | 86.445724 | 80.661377 | 84.552475 | 94.240105 | 94.134789 |
| 90 | 89.067719 | 83.273926 | 86.692322 | 95.559105 | 97.487801 |
| 100 | 89.781746 | 84.064789 | 89.211945 | 97.580551 | 99.588539 |

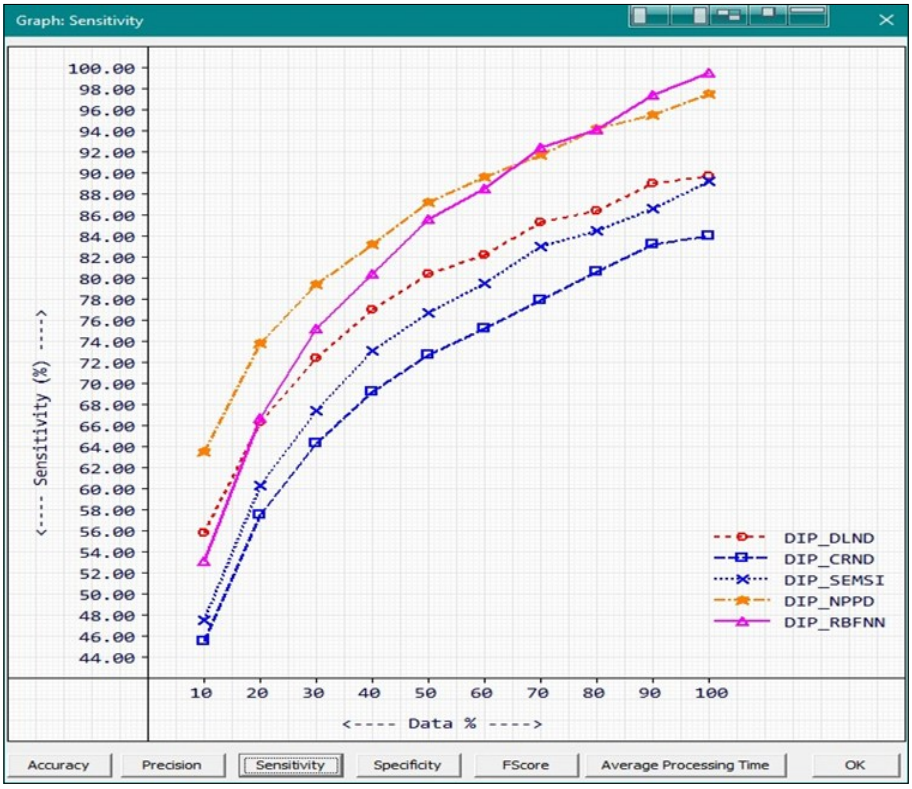


**Fig. 9.** Sensitivity chart.

**Table 4.** Experimental specificity (%)

| Data (%) | DIP_DLND | DIP_CRND | DIP_SEMSI | DIP_NPPD | DIP_RBFNN |
|---|---|---|---|---|---|
| 10 | 55.867607 | 45.510845 | 47.4883 | 63.592648 | 53.062027 |
| 20 | 66.803467 | 57.472656 | 60.445953 | 73.827667 | 67.111137 |
| 30 | 73.240448 | 63.968414 | 67.196815 | 79.713341 | 74.792305 |
| 40 | 76.633606 | 68.778488 | 72.909966 | 83.901711 | 81.098389 |
| 50 | 80.304367 | 72.373116 | 76.458893 | 86.492699 | 84.896309 |
| 60 | 82.819702 | 75.56916 | 80.368416 | 89.999786 | 89.280411 |
| 70 | 84.839455 | 78.594223 | 82.972046 | 91.369133 | 92.467155 |
| 80 | 86.665054 | 79.874405 | 84.830002 | 93.364067 | 94.134789 |
| 90 | 88.524574 | 82.745758 | 86.987045 | 96.016983 | 97.487801 |
| 100 | 90.423386 | 83.524078 | 90.325462 | 97.107117 | 98.606583 |

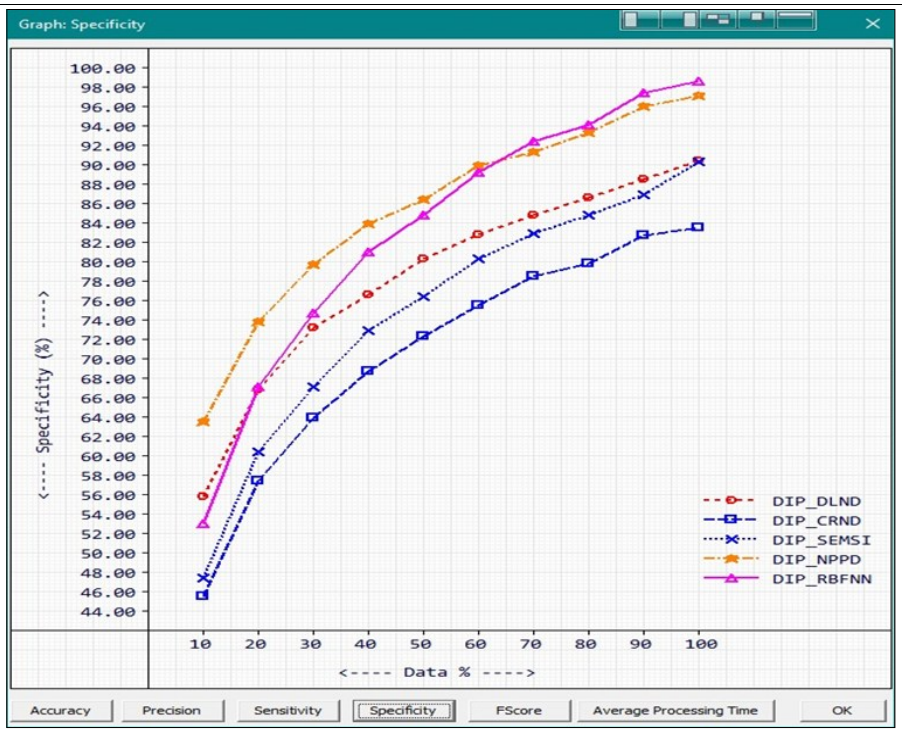


**Fig. 10.** Specificity chart.

As shown in Table 5 and Fig. 11, it is observed that when the data chunk exceeds 70 %, the F-score of the proposed method (DIP_RBFNN) improves by 8.91 % compared to the DIP_DLND, 16.37 % compared to DIP_CRND, 10.66 % compared to DIP_SEMSI and 1.24 % compared to DIP_NPPD for the PlantVillage dataset.

As shown in Table 6 and Fig. 12, it is observed that the differences in the average processing times of the proposed DIP_RBFNN compared to the DIP_DLND, DIP_SEMSI and DIP_NPPD method are 100 ms, 55 ms and 595 ms respectively.

The confusion matrix for the proposed model is depicted in Fig. 13, which evaluates the proposed model's performance by comparing the model's strength in image classification.

Fig. 14 depicts the diagnostic ability of the proposed system (binary classifier) as its discrimination threshold varies. The learning rate of the proposed system converges at around 0.26 and becomes saturated beyond the 0.7 threshold value.

## Conclusion

The proposed work handles the detection of nutrient deficiency in plant leaves using RBFNN. FHE was used for initial pre-processing of the plant leaf image dataset to extract image features. The processed images are filtered using the MAKF and the filtered images are trained and tested using RBFNN to find and classify nutrient (N, P, K) deficient plant leaves. The proposed method has been evaluated and simulation results prove that the accuracy, precision, specificity, sensitivity and F-score are better than the existing DIP_DLND, DIP_CRND, DIP_SEMSI and DIP_NPPD methods. The average processing time consumed to detect nutrient deficiency by the proposed method is 1951.1 ms. At the end of 100 % dataset processing, the True Positive Rate achieved is 98.59 %. While comparing the average processing time, the DIP_CRND method shows a better timing value than the proposed method, whereas all the remaining five performance metrics show over 16 % improved performance. Future research can be extended to improve the

**Table 5.** Experimental F-score (%)

| Data (%) | DIP_DLND | DIP_CRND | DIP_SEMSI | DIP_NPPD | DIP_RBFNN |
|---|---|---|---|---|---|
| 10 | 55.916126 | 45.732212 | 47.746048 | 63.592648 | 52.85693 |
| 20 | 66.800819 | 57.361889 | 60.4832 | 73.827667 | 67.1045 |
| 30 | 73.064537 | 63.915455 | 67.201607 | 79.615738 | 74.914803 |
| 40 | 76.738625 | 68.819939 | 72.966331 | 83.64447 | 80.88298 |
| 50 | 80.345329 | 72.441872 | 76.547287 | 86.791588 | 85.17112 |
| 60 | 82.62664 | 75.475998 | 80.082687 | 89.825226 | 88.942886 |
| 70 | 85.030937 | 78.380814 | 82.996529 | 91.554871 | 92.467155 |
| 80 | 86.575195 | 80.133644 | 84.721245 | 93.766541 | 94.134789 |
| 90 | 88.754883 | 82.939491 | 86.865364 | 95.797401 | 97.487801 |
| 100 | 90.13945 | 83.72718 | 89.832085 | 97.335991 | 99.088097 |

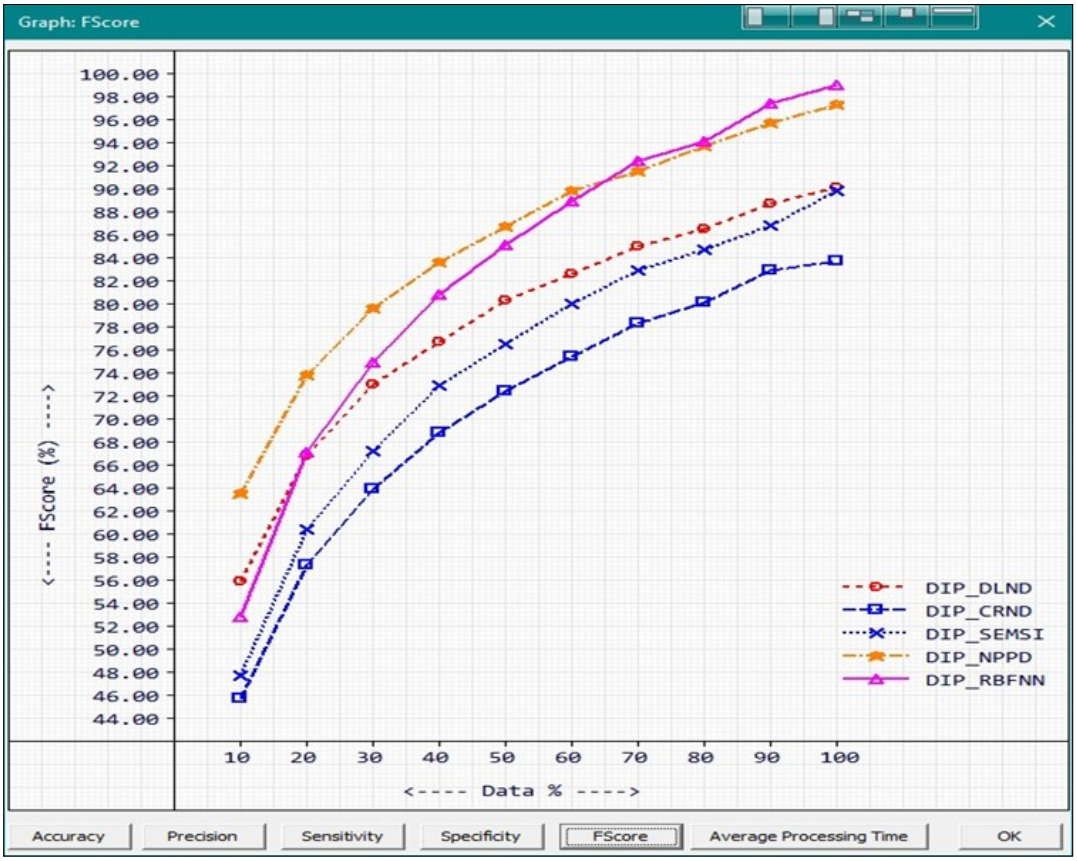


**Fig. 11.** F-score chart.

**Table 6.** Average processing time (ms)

| Data (%) | DIP_DLND | DIP_CRND | DIP_SEMSI | DIP_NPPD | DIP_RBFNN |
|---|---|---|---|---|---|
| 10 | 2144 | 1903 | 2004 | 2490 | 1958 |
| 20 | 2073 | 1839 | 1996 | 2454 | 1945 |
| 30 | 2121 | 1813 | 2068 | 2560 | 1952 |
| 40 | 2046 | 1831 | 1986 | 2470 | 1984 |
| 50 | 2048 | 1858 | 2102 | 2450 | 1910 |
| 60 | 2104 | 1815 | 2009 | 2451 | 1933 |
| 70 | 2181 | 1838 | 2046 | 2459 | 1897 |
| 80 | 2073 | 1868 | 2038 | 2569 | 1981 |
| 90 | 2083 | 1922 | 2101 | 2514 | 1970 |
| 100 | 2074 | 1875 | 2036 | 2571 | 1981 |

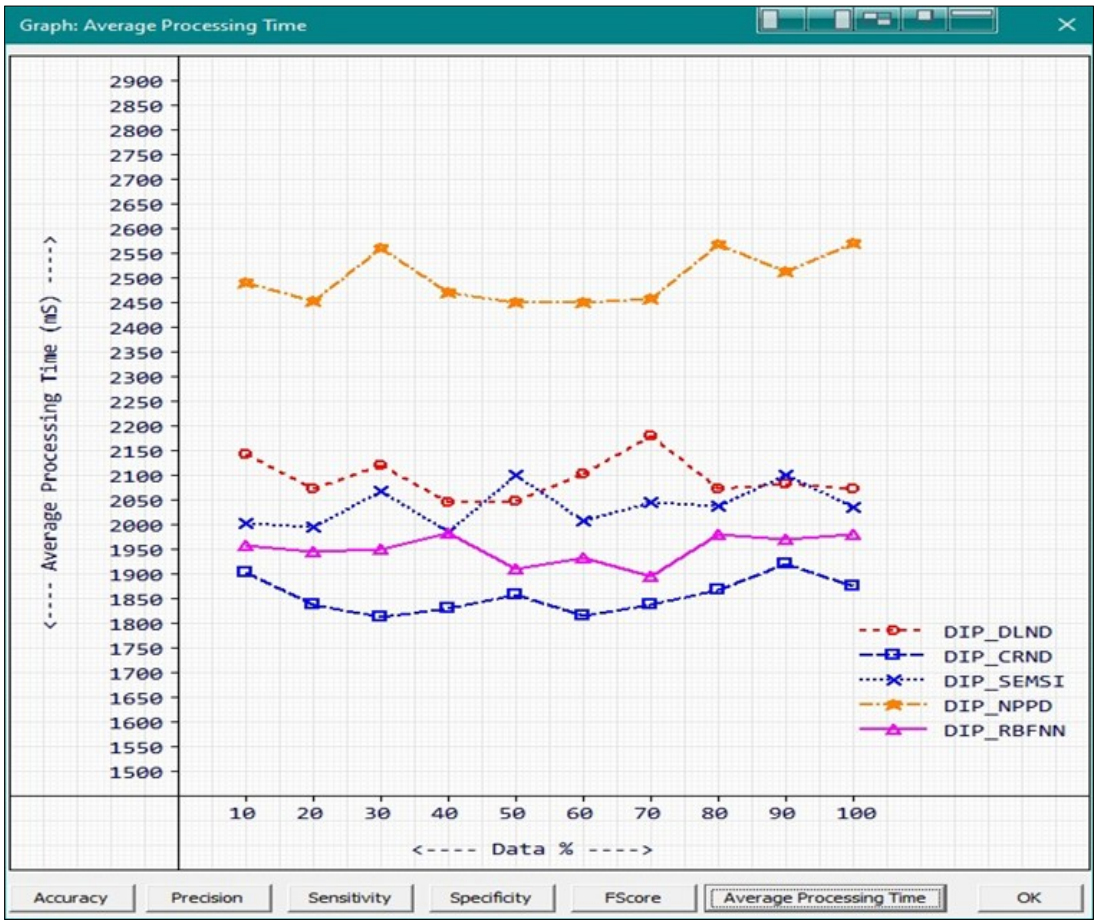


**Fig. 12.** Average processing time chart.

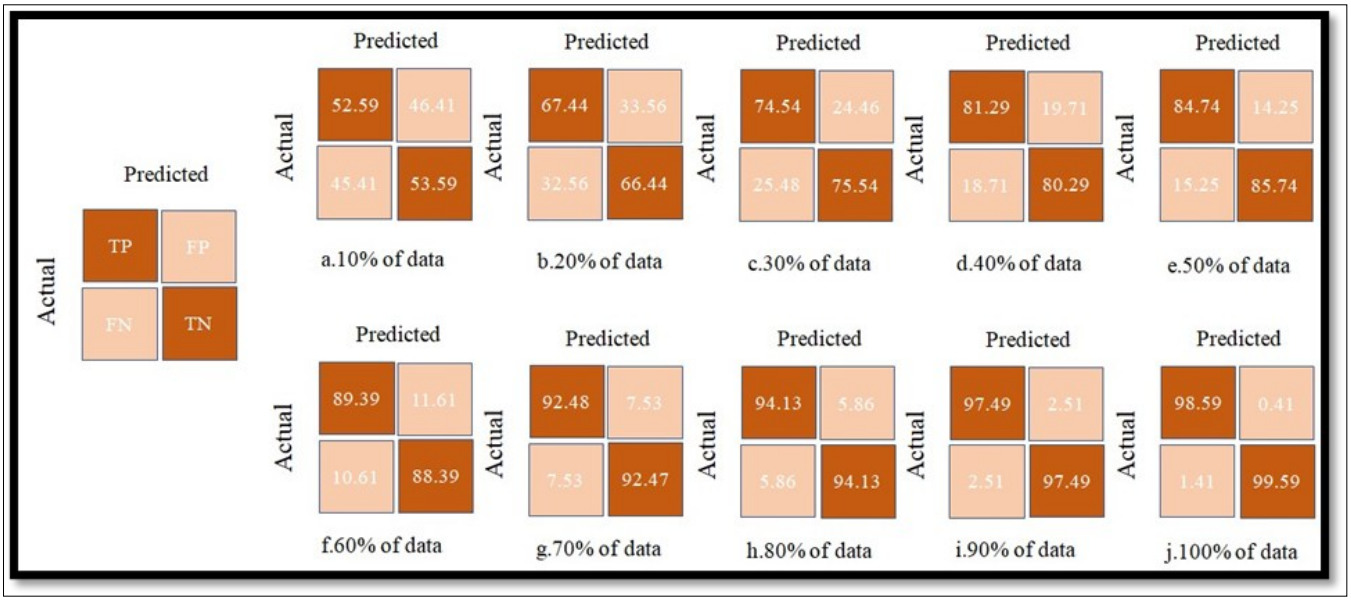


**Fig. 13.** Confusion matrix showing the percentage distribution of the dataset.

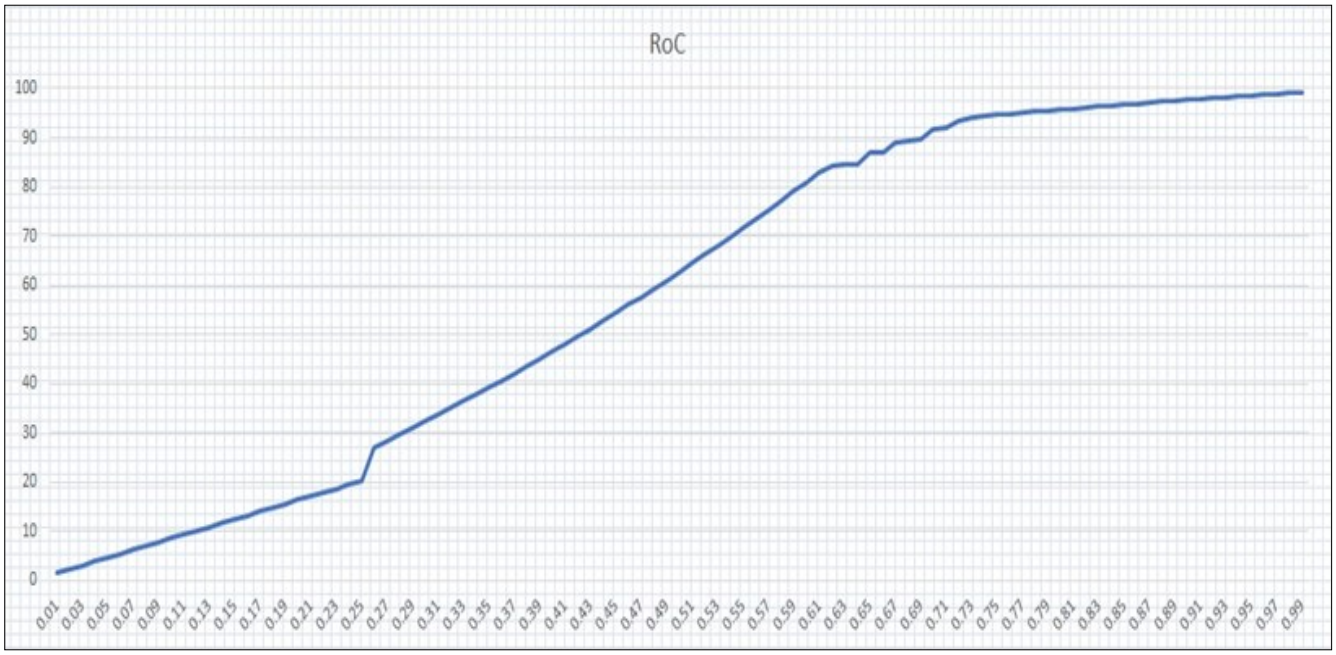


**Fig. 14.** ROC curve of the proposed model.

average processing time of the proposed RBFNN model. Parallelization and hardware acceleration, pruning and sparsity and approximate nearest-neighbour search are a few advanced methods to be attempted to improve the average processing time of the proposed RBFNN model in future research.

## Acknowledgements

The authors sincerely thank the International Plant Nutrition Institute (IPNI) and PlantVillage for providing the datasets. The nutrient-deficiency dataset from IPNI was augmented with the PlantVillage dataset to create the composite dataset used in this study.

## Authors' contributions

AS carried out the research under the guidance of PP. All authors read and approved the manuscript.

## Compliance with ethical standards

**Conflict of interest:** The authors declare that they have no conflicts of interest.

**Ethical issues:** None

## References

1. Passino KM. Biomimicry of bacterial foraging for distributed optimization and control. IEEE Control Systems Magazine. 2002;22 (3):52–67. https://doi.org/10.1109/MCS.2002.1004010
2. Strange RN, Scott PR. Plant disease: A threat to global food security. Annual Review of Phytopathology. 2005;43(1):83–116. https://doi.org/10.1146/annurev.phyto.43.113004.133839
3. Barbedo JG. Detection of nutrition deficiencies in plants using proximal images and machine learning: A review. Computers and Electronics in Agriculture. 2019;162:482–92. https://doi.org/10.1016/j.compag.2019.04.035
4. Azimi S, Kaur T, Gandhi TK. A deep learning approach to measure stress level in plants due to nitrogen deficiency. Measurement. 2021;173:108650. https://doi.org/10.1016/j.measurement.2020.108650
5. Elvanidi K, Augoustaki L. Crop reflectance measurements for nitrogen deficiency detection in a soilless tomato crop. Biosystems Engineering. 2018;176:1–11. https://doi.org/10.1016/j.biosystemseng.2018.09.019
6. Rustioni L, Grossi D, Brancadoro L, Failla O. Iron, magnesium, nitrogen and potassium deficiency symptom discrimination by reflectance spectroscopy in grapevine leaves. Scientia Horticulturae. 2018;241:152–9. https://doi.org/10.1016/j.scienta.2018.06.097
7. Chouhan SS, Kaul A, Singh UP, Jain S. Bacterial foraging optimization based radial basis function neural network (BRBFNN) for identification and classification of plant leaf diseases: An automatic approach towards plant pathology. IEEE Access. 2018;6:8852–63. https://doi.org/10.1109/ACCESS.2018.2800685
8. Montes Condori RH, Romualdo LM, Martinez Bruno O, de Cerqueira Luz PH. Comparison between traditional texture methods and deep learning descriptors for detection of nitrogen deficiency in maize crops. In: 2017 Workshop of Computer Vision; 2017. p. 7–12. https://doi.org/10.1109/WVC.2017.00009
9. Hairuddin MA, Tahir NM, Baki SR. Overview of image processing approach for nutrient deficiencies detection in *Elaeis guineensis*. In: Proceedings of IEEE International Conference on System Engineering and Technology; 2011. p. 116–20. https://doi.org/10.1109/ICSEngT.2011.5993432
10. Noh H, Zhang Q. Shadow effect on multi-spectral image for detection of nitrogen deficiency in corn. Computers and Electronics in Agriculture. 2012;83:52–7. https://doi.org/10.1016/j.compag.2012.01.014
11. Romualdo LM, Luz PH, Devechio FF, Marin MA, Zúñiga AM, Bruno OM, et al. Use of artificial vision techniques for diagnostic of nitrogen nutritional status in maize plants. Computers and Electronics in Agriculture. 2014;104:63–70. https://doi.org/10.1016/j.compag.2014.03.009
12. Shah A, Gupta P, Ajgar YM. Macro-nutrient deficiency identification in plants using image processing and machine learning. In: Proceedings of 3rd International Conference for Convergence in Technology; 2018. p. 1–4. https://doi.org/10.1109/I2CT.2018.8529789

13. Zermas D, Nelson HJ, Stanitsas P, Morellas V, Mulla DJ, Papanikolopoulos N. A methodology for the detection of nitrogen deficiency in corn fields using high-resolution RGB imagery. IEEE Transactions on Automation Science and Engineering. 2021;18 (4):1967–77. https://doi.org/10.1109/TASE.2020.3022868

14. Moghe R, Zanetti R, Akella MR. Adaptive Kalman filter for detectable linear time-invariant systems. Journal of Guidance, Control and Dynamics. 2019;42(8):1767–75. https://doi.org/10.2514/1.G004359

15. Huang Y, Zhang Y, Wu Z, Li N, Chambers J. A novel adaptive Kalman filter with inaccurate process and measurement noise covariance matrices. IEEE Transactions on Automatic Control. 2018;63(2):594–601. https://doi.org/10.1109/TAC.2017.2730480

16. Zidan KA, Jumaa SS. Finger vein recognition using two parallel enhancement approaches based fuzzy histogram equalization. Periodicals of Engineering and Natural Sciences. 2019;7(1):514–29. https://doi.org/10.21533/pen.v7i1.434

17. Mirbolouk S, Valizadeh M, Amirani MC, Choukali MA. A fuzzy histogram weighting method for efficient image contrast enhancement. Multimedia Tools and Applications. 2021;80(2):2221-41. https://doi.org/10.1007/s11042-020-09801-w

18. Magudeeswaran V, Ravichandran CG. Fuzzy logic-based histogram equalization for image contrast enhancement. Mathematical Problems in Engineering. 2013;2013:891864. https://doi.org/10.1155/2013/891864

19. Sun Y, Tong C, He S, Wang K, Chen L. Identification of nitrogen, phosphorus and potassium deficiencies based on temporal dynamics of leaf morphology and colour. Sustainability. 2018;10 (3):762. https://doi.org/10.3390/su10030762

20. Hassan SK, Maji AK, Jasiński M, Leonowicz Z, Jasińska E. Identification of plant-leaf diseases using CNN and transfer-learning approach. Electronics. 2021;10(12):1388. https://doi.org/10.3390/electronics10121388

21. Mukherjee A. Analysis of diseased leaf images using digital image processing techniques and SVM classifier and disease severity measurements using fuzzy logic. International Journal of Science and Engineering Research. 2020;11(8):1905–12. https://doi.org/10.14299/ijser.2020.08.12

22. Chouhan SS, Kaul A, Singh UP. Radial basis function neural network for the segmentation of plant leaf disease. In: Proceedings of 4th International Conference on Information Systems and Computer Networks; 2019. p. 713–6. https://doi.org/10.1109/ISCON47742.2019.9036299

23. Oskoei AM. Adaptive Kalman filter applied to vision based head gesture tracking for playing video games. Robotics. 2017;6(4):33. https://doi.org/10.3390/robotics6040033

24. Naikwadi S, Amoda N. Advances in image processing for detection of plant diseases. International Journal of Applied Innovation in Engineering and Management. 2013;2(11):206–12.

## Additional information

**Peer review**: Publisher thanks Sectional Editor and the other anonymous reviewers for their contribution to the peer review of this work.

**Reprints & permissions information** is available at https://horizonepublishing.com/journals/index.php/PST/open_access_policy

**Publisher's Note**: Horizon e-Publishing Group remains neutral with regard to jurisdictional claims in published maps and institutional affiliations.

**Indexing**: Plant Science Today, published by Horizon e-Publishing Group, is covered by Scopus, Web of Science, BIOSIS Previews, Clarivate Analytics, NAAS, UGC Care, etc
See https://horizonepublishing.com/journals/index.php/PST/indexing_abstracting



**Publisher information:** Plant Science Today is published by HORIZON e-Publishing Group with support from Empirion Publishers Private Limited, Thiruvananthapuram, India.